ACS Catalysis

Research Article

pubs.acs.org/acscatalysis

Surface Diastereomeric Complexes Formed by Methyl Benzoylformate and (*R*)-1-(1-Naphthyl)ethylamine on Pt(111)

Guillaume Goubert and Peter H. McBreen*

Centre in Green Chemistry and Catalysis, Department of Chemistry, Université Laval, Québec G1V 0A6, Canada

ABSTRACT: The formation of diastereomeric complexes between methyl benzoylformate (MBF) and (*R*)-1-(1-naphthyl)-ethylamine, (*R*)-NEA, on Pt(111) was studied using scanning tunneling microscopy. We observe several distinct geometries formed by 1:1 and 2:1 MBF/(*R*)-NEA complexes. The complexation patterns are compared with our previous data for 2,2,2-trifluoroacetophenone, (TFAP)/(*R*)-NEA, and methyl-3,3,3 trifluoropyruvate, (MTFP)/(*R*)-NEA, complexes on Pt(111). Steric hindrance due to the phenyl group forces MBF to form complexes that are inverted relative to those formed by MTFP. Compared to TFAP, the addition of the ester group, permitting intermolecular bonding through either the ester or the keto-carbonyl or both, increases the number of complexation geometries that the substrate can adopt. In particular, the ketoester group permits the phenyl group to be placed distant from (*R*)-NEA at several positions while also permitting NH···OC bonding. Overall, this leads to a decrease of the prochiral selectivity relative to TFAP/(*R*)-NEA complexes.

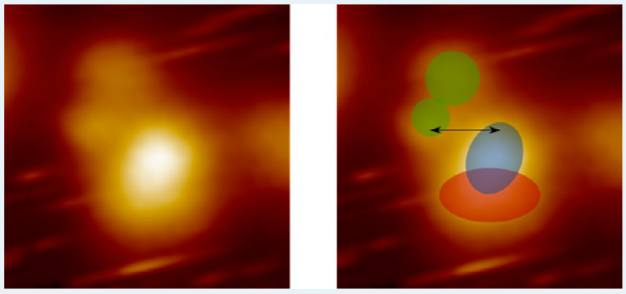

KEYWORDS: *asymmetric hetrogeneous hydrogenation, chemisorption, scanning tunneling microscopy, Orito reaction, chiral induction, α-ketoesters, methyl benzoylformate*

INTRODUCTION

Orito and co-workers reported the heterogeneously catalyzed enantioselective hydrogenation of methyl benzoylformate (MBF) to methyl mandelate in the first papers on the hydrogenation of α-ketoesters on cinchona-modified Pt catalysts.[1] Several groups[2] subsequently studied this reaction, and ee as high as 98% were reported.[2a] The reaction mechanism is believed to involve 1:1 complexation between the chiral modifier and the substrate on the metal surface prior to hydrogenation.[3] In this description, the modifier forms isolated chiral sites at which diffusing substrate molecules are captured. At these sites, the adsorbed substrate is preorganized such that either the *re* or *si* enantioface is preferentially turned toward the surface, thereby biasing the prochiral ratio on the surface. As illustrated in Scheme 1, a pro-R MBF adsorbate is defined as one that would yield (*R*)-methyl mandelate upon addition of a hydrogen atom at the enantioface in contact with the Pt(111) surface. A pro-S molecule in the same conditions would be hydrogenated into (*S*)-methyl mandelate.

In previous work, we used scanning tunneling microscopy (STM) and density functional theory (DFT) methods to study the preorganization of two different prochiral substrates, 2,2,2-trifluoroacetophenone (TFAP) and methyl-3,3,3 trifluoro-pyruvate (MTFP), on (*R*)-1-(1-naphthyl)ethylamine, (*R*)-NEA, modified Pt(111).[4,5] We demonstrated that in cases where STM images of modifier−substrate complexes display clear submolecular resolution, detailed regiospecific and stereospecific information could be obtained by comparison to systematic DFT searches for the most stable complexes. For both TFAP and MTFP, a number of binding sites were observed around the ethylamine group of individual (*R*)-NEA molecules, showing that the modifier presents several competing chiral pockets. It was possible to determine prochiral ratios specific to individual chiral pockets, and to relate this information to the stereodirecting interactions operating at individual sites. In this way, a hierarchy of intermolecular and chemisorption interactions underlying prochiral selection was established for both substrates. Under purely thermodynamic control, the prochiral ratio of the adsorbed substrate would lead to a corresponding enantiomeric ratio in the hydrogenation product. However, because we lack information on the kinetics of hydrogenation in the different complexes, it is not possible to predict enantioselectivies from the prochiral ratios determined in the STM experiments.

The formation of MBF/(*R*)-NEA complexes on Pt(111) was studied solely using STM measurements. In order to interpret the data, we exploit the fact that MBF contains a phenyl group and a ketoester moiety and hence combines key structural elements from TFAP and MTFP. The latter two molecules were found to present significantly different complexation patterns when interacting with (*R*)-NEA. For TFAP/(*R*)-NEA,[4] chemisorption of the phenyl group in a bridge site, η^2-chemisorption of the carbonyl group, and substrate-modifier NH···OC bonding dominate the stabilization of complexes.

Received: September 24, 2013
Revised: December 15, 2013
Published: January 31, 2014

Scheme 1. Schematic Illustration of the Formation of Pro-R and Pro-S Adsorbed States of Methyl Benzoylformate (MBF), and Pt-Catalyzed Hydrogenation to Yield (*R*) and (*S*)-Alcohol Desorption Products

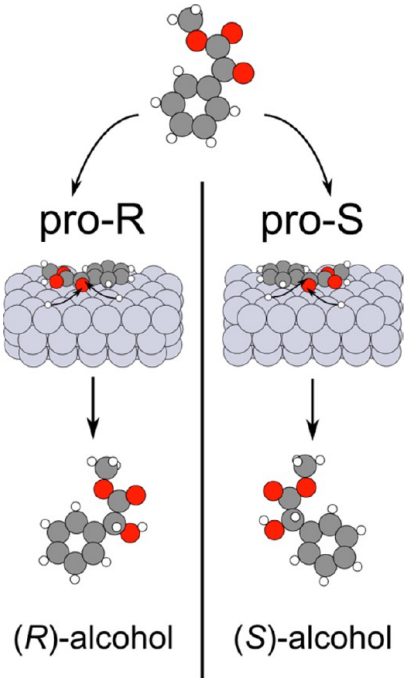

Steric interactions involving the phenyl group determine the prochiral ratio of TFAP at a given site. A significant difference arises for MTFP, in that its two carbonyls can form attractive interactions with the modifier[5] and in that it does not possess a strongly chemisorbed phenyl group. The most stable structure found for MTFP/(*R*)-NEA involves NH···OC bonding to the ester-carbonyl and NH···OC and CH···OC bonding to the keto-carbonyl, in addition to η^2-chemisorption of the keto-carbonyl group. In the present study, we are particularly interested in the effect of the combination of a phenyl ring and two hydrogen bond acceptors on the complexation of MBF to (*R*)-NEA. As for the experiments on MTFP and TFAP, the experiments on MBF were performed at room temperature so as to obtain information of as much relevance as possible to actual reaction conditions. The enantioselective hydrogenation of MBF on chirally modified Pt catalysts is typically carried between 0 °C and room temperature.[2]

In this study, we seek to demonstrate that in cases where sufficiently detailed molecular information is already available for related systems, as for TFAP/(*R*)-NEA and MTFP/(*R*)-NEA on Pt(111), it is possible to extrapolate this information to closely related systems such as MBF/(*R*)-NEA. That is, the aim is to extract information on the structure of MBF/(*R*)-NEA complexes by a visual inspection of the STM images. To do so, it is first necessary to recognize the molecular information contained in images of (*R*)-NEA (Figure 1). In our previous work,[4] we have shown that (*R*)-NEA adsorbs into two rotameric forms on Pt(111) in a population ratio of approximately 7:3. We label the majority conformer (*R*)-NEA-1 and the minority conformer (*R*)-NEA-2. They primarily differ in which face of the naphthyl group is turned toward the surface. Then, considering rotation of the ethylamine group for each conformer, the most stable (*R*)-NEA-1 geometry is an *exo*-conformer (where the amine points away from the naphthyl ring), and the most stable (*R*)-NEA-2 geometry is an *endo*-conformer (where the amine points toward the nonsubstituted ring). In both cases, when looking down on the adsorbed molecule as it is drawn in the middle panel of Figure 1, the amine group is pointing to the right-hand side. In the STM images of (*R*)-NEA, a bright protrusion is observed at the position of the ethylamine moiety, and an oval and dimmer shape is assigned to the naphthyl group. Similar conclusions were drawn by Tysoe et al. in their STM, vibrational spectroscopy, and DFT studies for NEA on Pd(111).[6]

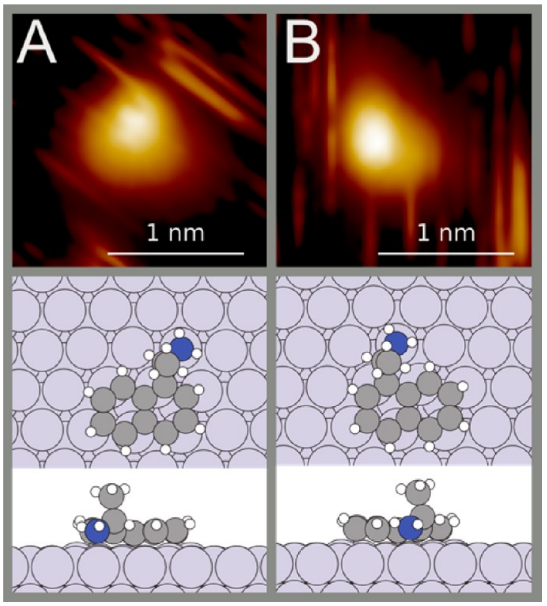

Figure 1. (A, B) Previously published[4] STM images and DFT-calculated structures of (*R*)-NEA-1 and (*R*)-NEA-2 on Pt(111). Adapted with permission from ref 4. Copyright 2011 The American Association for the Advancement of Science.

EXPERIMENTAL SECTION

The STM experiments were carried out in an ultrahigh vacuum (UHV) chamber equipped with a SPECS Aarhus STM-150 microscope. All images were acquired at room temperature at a constant tunneling current in the 0.15−0.33 nA range and a bias voltage in the 0.9−1.1 V range. WSxM image treatment software was used to adjust brightness and contrast.[7] The Pt(111) crystal (MaTecK Gmbh) was cleaned by cycles of Ar^+ ion bombardment at 600 K and oxygen (2×10^{-7} Torr) treatment at 900 K followed by flash annealing to 1050 K. Methyl benzoylformate (MBF, 97% purity) and (*R*)-(+)-1-(1-naphthyl)ethylamine ((*R*)-NEA, 99% purity) were purchased from Sigma-Aldrich and further purified by pumping and freeze−thaw cycles in the gas handling vacuum line prior to introduction into the vacuum chamber.

RESULTS AND DISCUSSION

STM images of MBF on Pt(111) at room temperature show different types of dimers (Figure 2B−D), although monomers (Figure 2A) are rarely observed. Dimers 2 C and 2 D are fluxional and can interconvert over the course of an experiment. A sequence of images showing this behavior is presented in Figure 3. We propose that the fluxionality arises through rotational freedom of the ketoester moiety and the fact that MBF possesses a number of H-bond acceptors, thereby permitting combinations of intermolecular bonding config-

dx.doi.org/10.1021/cs400846j | ACS Catal. 2014, 4, 847−854

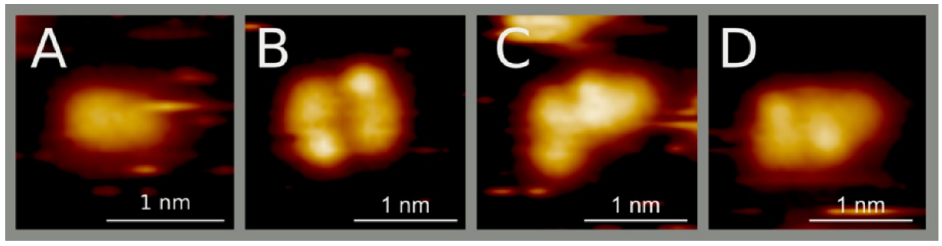

Figure 2. STM images of MBF on Pt(111) at room temperature. (A) Monomer MBF; (B–D) MBF dimers.

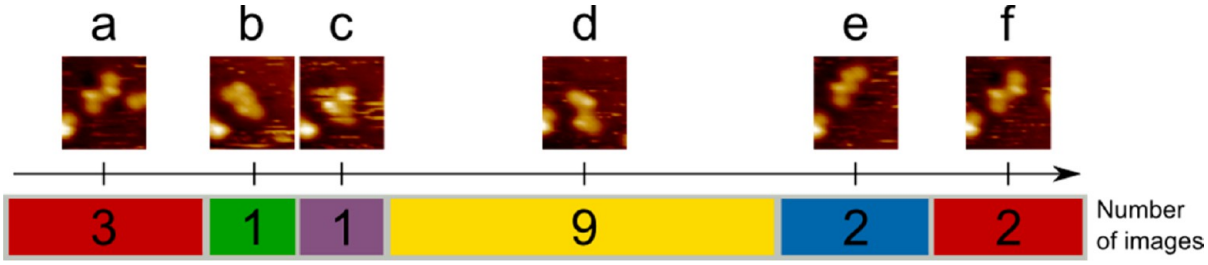

Figure 3. Time-lapsed sequence of images of a MBF dimer showing interconversion between different geometries (a–f). The numbers within the colored segments of the bar indicate the number of sequential images in which the corresponding dimer configuration is seen. The measurements were performed at room temperature, and each image was acquired in 44 s.

urations. Dimer 2 B, in contrast, is not observed to convert to other geometries during experiments. By reference to our previous studies of interactions of oxygenates with aromatic molecules on Pt(111), we propose that multiple aryl-CH···OC bonding occurs in dimer 2 B. The stability of dimer 2 B is then attributed to the formation of closed structures such as those schematically illustrated in Scheme 2 where either *cis*-MBF or *trans*-MBF molecules are counter-aligned and each forms a CH···OC bond between a carbonyl and the phenyl group of the other molecule.

Scheme 2. Schematic Drawing of Plausible Dimer Structures Corresponding to the Dimer Image Shown in Figure 2B

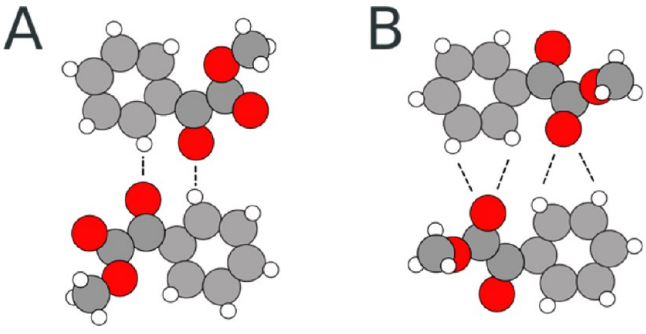

Representative STM images for MBF/(*R*)-NEA are shown in Figure 4. The experiments were performed by first exposing the Pt(111) surface to (*R*)-NEA and then dosing MBF. All parts of the experiments were carried out at ambient temperature. A distribution of distinct 1:1 MBF/(*R*)-NEA (Figure 4A–E,G,H,J) and termolecular, $(MBF)_2$/(*R*)-NEA, (Figure 4F,I) complexes were observed. MBF in complexes is imaged as an elongated shape with the end of the molecule in contact with (*R*)-NEA being smaller in width. We label the smaller end of the protrusion as the head. We can then define a direction to MBF molecules along the long axis, oriented from the larger part of the protrusion to the head. On the basis of our previous analysis of complexes formed by TFAP or MTFP and (*R*)-NEA, we can safely assume that the MBF/(*R*)-NEA complexes shown in Figure 4 all involve NH···OC bonding. Hence, we assign the head of the MBF image as the ketoester moiety, as it forms the contact to (*R*)-NEA, and the larger protrusion as the phenyl moiety. In this context, we note that Baiker et al. have shown using a sensitive in situ vibrational technique that MBF forms NH···OC bonded complexes to protonated cinchonidine on supported Pt.[3a]

As a first step in categorizing the substrate/(*R*)-NEA complexes, we draw the modifier with the long axis of the naphthyl group along the horizontal and the ethylamine group pointing upward. Complexes can then be first categorized into structures where the substrate is located to the top, to the left, or to the right-hand side of the ethylamine group (bright protrusion) of (*R*)-NEA (Figure 5 and Table 1). The first observation that emerges from such a categorization of a sample of 350 complexes is that MBF is located to the right-hand side in the majority of complexes formed by both conformers of (*R*)-NEA. MBF is located to the right-hand side of the ethylamine group in ∼60% of the (*R*)-NEA-2 complexes and in ∼74% of the (*R*)-NEA-1 complexes. For (*R*)-NEA-2, approximately half of the structures in which binding on the left-hand side occurs are termolecular, $(MBF)_2$/(*R*)-NEA, complexes (Figure 4F). Similarly, for (*R*)-NEA-1 a third of the left-hand-side binding occurs in termolecular complexes (Figure 4I), suggesting that the right-hand sites are preferentially filled.

As a second step in categorizing the complexes, it is possible to identify recurrent STM motifs of MBF /(*R*)-NEA complexes at the right, left and top of the ethylamine group. For example, it can be seen from Figure 4 that there are several different structures formed by MBF binding to the right-hand side of (*R*)-NEA-2. Complexes are found with the orientation of MBF ranging from approximately 10° (Figure 4I) to approximately 90° (Figure 4G) relative to the naphthyl axis. The images shown in Figure 4G,I are representative of families of right-hand-side complexes. Complexes where MBF displays a spread of intermediate orientations are also found, but they are not included in Figure 4, because they cannot be readily assigned to

dx.doi.org/10.1021/cs400846j | *ACS Catal.* 2014, 4, 847–854

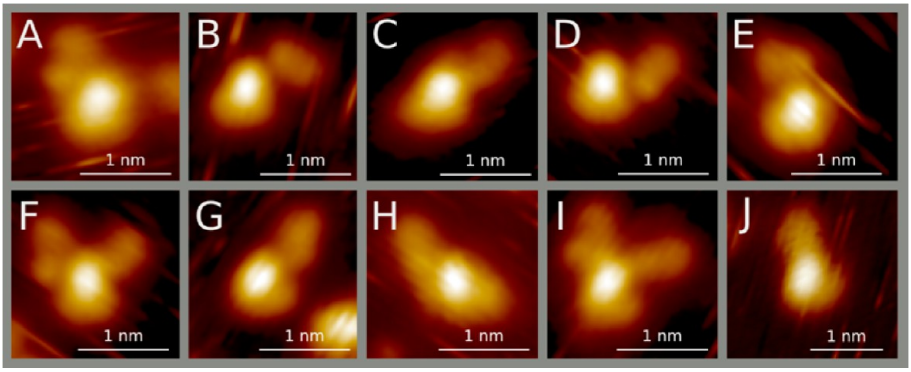

Figure 4. STM images of (*R*)-NEA/MBF complexes formed on Pt(111) at room temperature. MBF forms complexes mainly on the right-hand side of the bright protrusion of (*R*)-NEA, as shown in (B–D, F) for (*R*)-NEA-1 and (G, I) for (*R*)-NEA-2. Complexes formed with MBF to the left-hand side of the bright protrusion are presented in (A, F) for (*R*)-NEA-1 and in (H, I) for (*R*)-NEA-2. Termolecular, $(MBF)_2/(R)$-NEA, complexes are shown in (F, I). Complexes where MBF is located at the top of the bright protrusion are presented in (E) for (*R*)-NEA-1 and in (J) for (*R*)-NEA-2.

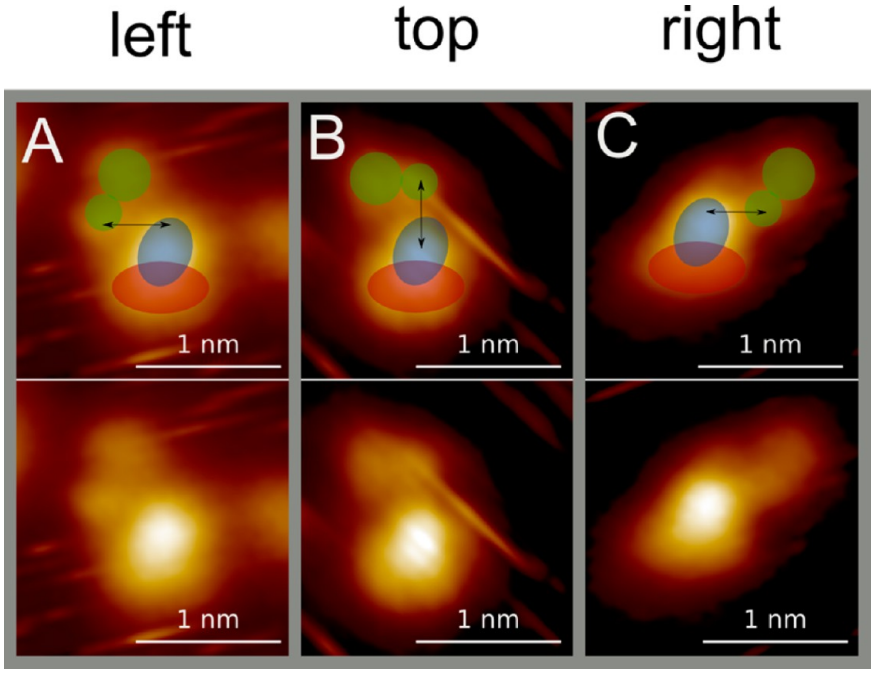

Figure 5. Primary classification of complexes into structures formed by MBF binding to the left, top, or right of (*R*)-NEA. Structures (A–C) (shown in both the top and bottom panels) are three different MBF/(*R*)-NEA-1 complexes. The bright protrusion locates the ethylamine group of the modifier. The top panel includes a color scheme as a guide to the eye. The red oval indicates the naphthyl group. The blue oval indicates the ethylamine group. The MBF molecule is indicated in green, with the narrow and wide ends of the image differentiated. The black arrow connecting the head of MBF and the ethylamine group schematically indicates an NH···OC bond.

Table 1. Relative Abundances of Left-, Top- and Right-Hand Side Binding Geometries in a Sample of 350 MBF/(*R*)-NEA Complexes on Pt(111)

	left	top	right
(*R*)-NEA-1	15%	10%	74%
(*R*)-NEA-2	23%	17%	60%

single families. The MBF/(*R*)-NEA-1 images shown in Figure 4B–D are representative of families of complexes, but they also exist alongside complexes with other orientations. In total, the images shown in Figure 4 are representative of close to 60% of all of the observed complexes.

As outlined in the Introduction, we will attempt to interpret MBF/(*R*)-NEA complexation patterns by reference to our published results on TFAP/(*R*)-NEA[4] and MTFP/(*R*)-NEA complexes.[5] We take the DFT-calculated structures of the latter complexes and extrapolate from them what we believe are plausible structures for MBF/(*R*)-NEA, and compare the proposed structures to the present STM data. Such a comparative analysis of MTFP/(*R*)-NEA-2 and MBF/(*R*)-NEA-2 right-hand-side complexes is presented in Figure 6. We first summarize the published MTFP data.[5] STM images that match simulated images for the two most stable DFT-calculated MTFP/(*R*)-NEA-2 complexes are shown in Figure 6A,B. Structure 6A is the most stable MTFP/(*R*)-NEA-2 complex found in the DFT calculations, and it corresponds well with the most abundant complex observed by STM. Structure 6B is the second most stable DFT-calculated MTFP/(*R*)-NEA-2 structure, and STM images that correlate well with it are only observed when the sample is cooled from room temperature. Structures C and D are still less stable DFT-calculated MTFP/

dx.doi.org/10.1021/cs400846j | *ACS Catal.* 2014, 4, 847–854

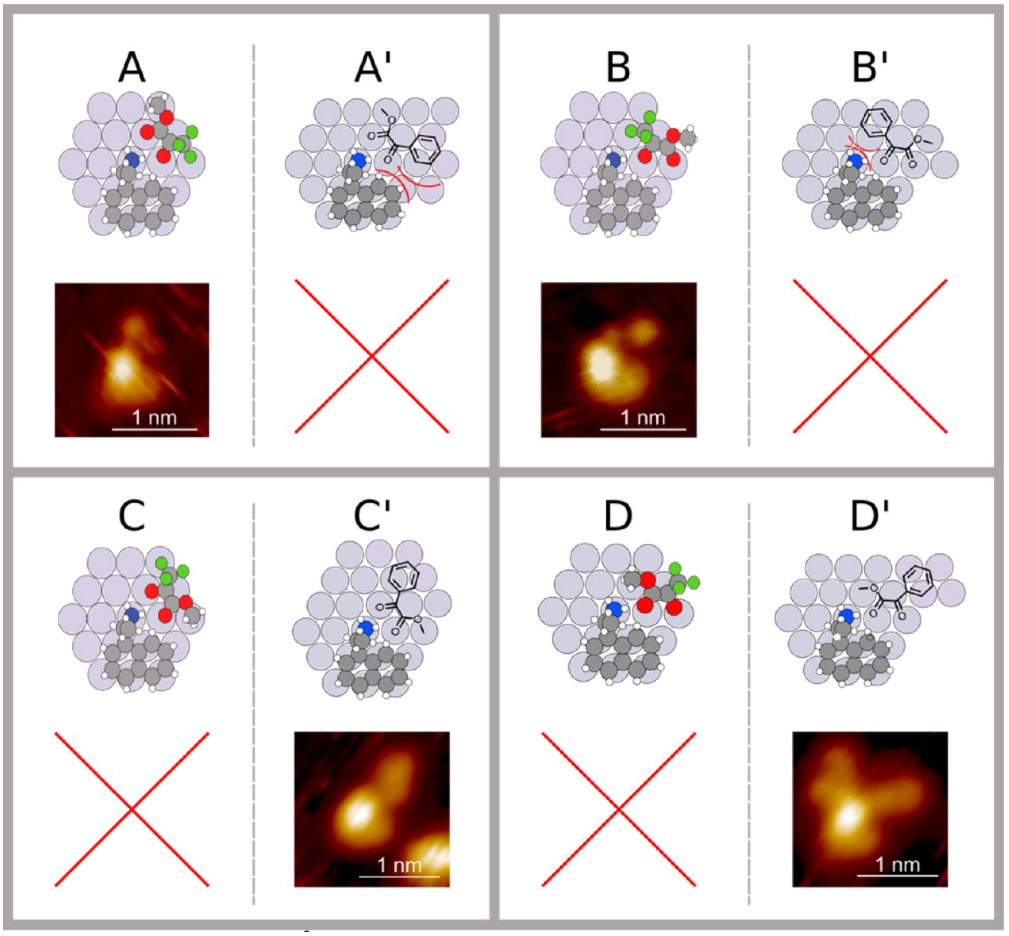

Figure 6. Comparison of published[5] DFT-calculated structures (A–D) and STM images (A, B) for MTFP/(*R*)-NEA-2 complexes with proposed structures (A′–D′) and STM images (C′, D′) for MBF/(*R*)-NEA-2 right-hand-side complexes. A red X indicates a structure that is not observed in STM measurements. Proposed MBF/(*R*)-NEA-2 structures are drawn by replacing the CF_3 group of the corresponding MTFP structure with a phenyl group. Structures A, A′, B, and B′ differ from structures C, C′, D, and D′, respectively, in terms of the enantioface of the substrate that is directed toward the surface.

(*R*)-NEA-2 complexes. They differ from complexes A and B in terms of the prochirality of the substrate (as defined in Scheme 1). That is, the substrate is flipped over on going from A to C and from B to D. The calculated published complexation energies of the four MTFP/(*R*)-NEA-2 structures are as follows: A (0.64 eV), B (0.54 eV), C (0.51 eV), and D (0.36 eV).[5]

The proposed structures for MBF/(*R*)-NEA-2 complexes shown in Figure 6 are drawn by taking corresponding DFT-calculated MTFP/(*R*)-NEA-2 complexes and replacing the CF_3 group by a phenyl group. In structures A′–D′, the two carbonyl oxygen atoms of MBF are kept in the same positions as for the DFT-calculated MTFP complexes A–D. This approach is only schematic, because it does not systematically respect the preference of the phenyl group to occupy a bridge site, and because it does not describe the distances of the oxygen atoms above the surface. Nevertheless, it offers an explanation for the stark difference between the two sets of STM images (A versus C′ and B versus D′) in Figure 6. Notably, the STM images for MBF/(*R*)-NEA-2 (C′, D′) match the two least stable MTFP/(*R*)-NEA-2 complexes (C, D) rather than the two most stable ones (A, B). As illustrated in Figure 6A′,B′, we propose that the difference in binding geometries between MTFP/(*R*)-NEA-2 and MBF/(*R*)-NEA-2 complexes occurs to avoid steric repulsion between (*R*)-NEA-2 and the phenyl group of MBF.

The most stable MTFP/(*R*)-NEA-2 structure, 6A, and the MBF/(*R*)-NEA-2 structure proposed in 6C′ both involve two point/two carbonyl contact between the ketoester and the modifier. However, the specific carbonyl to (*R*)-NEA-2 interactions are inverted. Whereas structure A places the keto-carbonyl of MTFP in a position to form a combination of NH···OC and CH···OC bonding, the keto-carbonyl of MBF is hindered from forming an analogous set of interactions by unfavorable phenyl–naphthyl interactions and is not observed experimentally (as illustrated in 6A′). The results suggest that the ester-carbonyl of MBF preferentially docks in proximity of the NH and aryl-CH bonds while the keto-carbonyl interacts with an NH bond, so that the phenyl group points away from the chiral modifier (6C′). For both MTFP and MBF, less abundant pro-R structures (shown in Figure 6B,D) are formed by one point/one carbonyl contact. Again, in these structures, MBF is inverted relative to MTFP in that it is the ester-carbonyl of MBF (structure 6D′) rather than the keto-carbonyl (structure 6B) that interacts with the modifier.

A comparison of the present MBF/(*R*)-NEA data to the published[4] analysis of TFAP/(*R*)-NEA complexes shows that MBF displays a much greater propensity than TFAP to form complexes to the right-hand side of (*R*)-NEA-2 (Table 1). Right-hand-side TFAP/(*R*)-NEA-2 complexes account for only a small percentage of the total population of TFAP/(*R*)-NEA

dx.doi.org/10.1021/cs400846j | *ACS Catal.* 2014, 4, 847–854

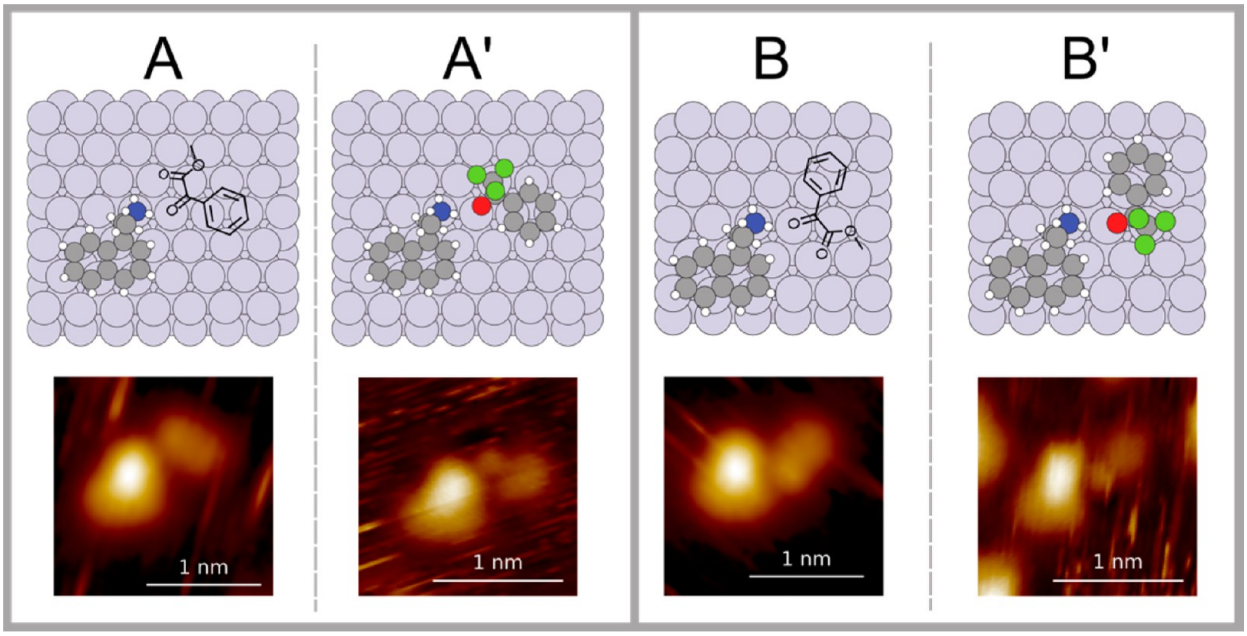

Figure 7. Comparison of STM images of right-hand-side MBF/(*R*)-NEA-1 (A, B) complexes to structures extrapolated from previously published STM and DFT-calculated data[4] on TFAP/(*R*)-NEA-1 complexes (A′, B′).

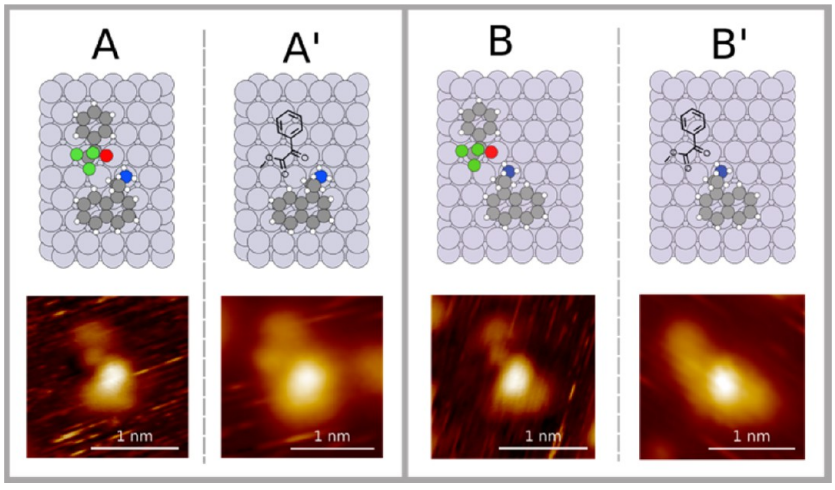

Figure 8. Comparison of STM images of left-hand-side MBF/(*R*)-NEA-1 (A′) and MBF/(*R*)-NEA-2 complexes (B′) to structures extrapolated from previously published STM and DFT-calculated data[4] on TFAP/(*R*)-NEA complexes (A, B).

complexes observed at room temperature, whereas the majority of MBF/(*R*)-NEA-2 complexes are found on the right-hand side (Figure 4F,G,I). We propose that, in contrast to TFAP, MBF can readily form right-hand-side complexes primarily because the ester moiety of MBF increases the distance between (*R*)-NEA-2 and the phenyl group. Complexes are then stabilized by strong adsorption of the phenyl group among other chemisorption interactions, plus an interaction of the ester-carbonyl with the modifier. In addition, the image shown in Figure 4D suggests that MBF/(*R*)-NEA-2 complexes involving both ester and keto-carbonyl bonding to the modifier are formed. We propose that in such complexes, the two-carbonyl interaction outweighs steric hindrance due to the phenyl group.

A comparison of images for TFAP/(*R*)-NEA-1 and MBF/(*R*)-NEA-1 right-hand-side complexes is shown in Figure 7. It shows strong similarities between the two sets of complexes. However, for TFAP/(*R*)-NEA-1, structure 7A′ is much more abundant than structure 7B′. In contrast, for MBF/(*R*)-NEA-1, structures 7A and 7B are of similar abundance. We propose that this arises either because for MBF structure 7B is stabilized through two-point/two-carbonyl bonding to (*R*)-NEA-1 or because both structures place the phenyl group of MBF distant from (*R*)-NEA-1 with the result that steric interactions are not important in differentiating between the two geometries.

Turning to complexes where MBF is captured to the left-hand side of (*R*)-NEA, we observe that STM images of both (*R*)-NEA-1 and (*R*)-NEA-2 complexes (Figure 8A′,B′, respectively) show that the substrate is oriented roughly perpendicular to the naphthyl axis. For (*R*)-NEA-2, this type of structure (Figure 8B′) is clearly dominant with very few complexes presenting a different geometry. For (*R*)-NEA-1 complexes, the selectivity is less pronounced with the geometry shown in Figure 8A′ accounting for roughly 40% of the population at this site. The MBF/(*R*)-NEA complexes shown in Figure 8A′,B′ can be best accounted for by using structures

dx.doi.org/10.1021/cs400846j | *ACS Catal.* 2014, 4, 847−854

similar to TFAP/(*R*)-NEA complexes (Figure 8A,B). This similarity arises because all of the structures shown in Figure 8 place the phenyl group distant from (*R*)-NEA. It is also important that these structures readily permit the phenyl group to occupy a bridge site.

An estimate of the overall prochiral ratios for MBF complexation at the left, top, and right sites of *(R)*-NEA can be attempted by extension of the above analysis. Under the assumption that all of the counted complexes involve NH···OC bonding (as illustrated in Figure 5), it is possible to establish the prochirality of complexed MBF if (i) the resolution of the STM images is sufficiently good to differentiate between the ketoester and phenyl groups of MBF and (ii) if we know whether the ketoester group is in the *cis* or *trans*-conformation. Vargas et al.[8] calculated the adsorption geometry of MBF on a Pt_{31} cluster model of Pt(111). They found that the most stable adsorption geometry, by almost 4 kcal/mol, is a *cis*-structure with the phenyl group in a bridge site and the keto-carbonyl η^2-bonded between two Pt atoms. Furthermore, DFT calculations for MTFP on Pt(111) show that *cis*-adsorption geometries, with the keto-carbonyl η^2-bonded, are over 4 kcal/mol more stable than *trans*-adsorption geometries.[5] Hence, in the following analysis, we assume that the ketoester group of MBF on Pt(111) is in the *cis*-conformation, although the MBF dimer images shown in Figure 3 suggest that *cis*−*trans* isomerization can occur. Within the assumption that MBF is in the *cis*-conformation, the quality of ∼70% of the images is sufficiently good to determine the prochirality of complexed MBF (as defined in Scheme 1). For example, Figure 4B,E show pro-R and pro-S MBF/(*R*)-NEA-1 complexes, respectively. Figure 4G,H show pro-S and pro-R MBF/(*R*)-NEA-2 complexes, respectively. The termolecular (*R*)-NEA-2 complex shown in Figure 4I involves pro-R MBF molecules in both the right and left-hand sites.

Estimated prochiral ratios for MBF/(*R*)-NEA complexes are presented in Table 2, keeping in mind that only 70% of the complexes are well enough resolved to make a determination of their prochirality. We find that the left-hand site is strongly biased toward pro-R MBF, in particular for (*R*)-NEA-2, whereas the top and right-hand sites are not selective or are weakly pro-S selective. The overall pro-R excess, counting all sites, is however small, because only a minority of complexes are formed to the left-hand side (Table 1). Focusing on the left-hand sites, the prochiral selectivity for MBF complexes is less than that previously found[4] for TFAP complexes. For MBF/(*R*)-NEA-1, the prochiral ratio is 3.7 compared to 11 for TFAP/(*R*)-NEA-1. For MBF/(*R*)-NEA-2, the prochiral ratio is 7 compared to 10 for TFAP/(*R*)-NEA-2. We propose that this lower selectivity for MBF, as compared to TFAP, arises because the phenyl group can be anchored relatively far from (*R*)-NEA, and the ketoester moiety can swing in toward the chiral molecule to form H-bond(s) involving either the ester-carbonyl or both carbonyls, without the phenyl group incurring steric repulsion. That is, the dominant interaction for TFAP and MBF, the chemisorption of the phenyl group, can occur in more positions for MBF while still permitting the formation of a NH···OC bond. We note that the highest complexation energy of MTFP to (*R*)-NEA (∼0.6 eV) is comparable to calculated barriers for the diffusion of benzaldehyde[9a] or TFAP[9b] out of bridge sites on Pt(111), and it is superior to the calculated energy difference (∼0.3 eV) between adsorption of TFAP at bridge and 3-fold sites. It is possible then that the adsorption of the phenyl group of complexed MBF is not limited to bridge sites, further increasing the number of stable binding geometries.

Table 2. Prochiral Ratios (pro-R/pro-S) for MBF Binding to the Left, Right, and Top of the Ethylamine Group of (*R*)-NEA

	left	top	right
(*R*)-NEA-1	3.7	1.1	0.5
(*R*)-NEA-2	7	0.7	0.8

On the basis of the prochiral ratios estimated from the STM data and on the assumption that kinetic factors do not play a role, the MBF/(*R*)-NEA system is predicted to show low enantioselectivity in hydrogenation on NEA-modified Pt catalysts. To the best of our knowledge, there is no catalysis data available to evaluate the quality of this prediction. It was noted in the Introduction that enantioselectivities of as high as 98% ee can be achieved in the hydrogenation of MBF on cinchonidine-modified Pt. The present study on MBF/(*R*)-NEA does not provide an explanation for the high stereoselectivity obtained using cinchonidine as the modifier.

As mentioned above, we have shown in previous work that TFAP displays a roughly equal propensity to form complexes with (*R*)-NEA-1 and (*R*)-NEA-2[4] and that MTFP displays a marked preference toward forming complexes with (*R*)-NEA-2.[5] MBF also displays a preference for (*R*)-NEA-2, although smaller than that for MTFP. These preferences imply that, in the presence of a solvent, MTFP and MBF would induce an increase in the ratio of (*R*)-NEA-2 to (*R*)-NEA-1 on the surface. In this context, we note reports in the literature[10,11] showing that under reaction conditions, α-ketoester substrates cause an inversion in the relative population of cinchonidine rotamers on Pt/Al_2O_3 catalysts. In elegant experiments, Baiker et al. showed that ethyl formate, ketopantolactone, and methyl benzoylformate all cause the relative populations of cinchonidine rotamers to invert.[10] Furthermore, they found no such effect using TFAP as the substrate.[11] Overall, our results on TFAP, MTFP, and MBF/(*R*)-NEA complexes measured under ultrahigh vacuum conditions correlate reasonably well with the observations by Baiker et al.[10,11]

CONCLUSIONS

STM measurements on diastereomeric complexes formed by MBF and (*R*)-NEA on Pt(111) at room temperature were compared with previously published[4,5] STM images and DFT-calculated structures for MTFP/(*R*)-NEA and TFAP/(*R*)-NEA complexes. This comparison centers on an analysis of how the combination of a phenyl group and a ketoester group in MBF changes the complexation patterns with respect to TFAP (which possesses a phenyl group but not an ester-carbonyl) and MTFP (which possesses a ketoester group but not a phenyl group). With respect to MTFP, MBF forms significantly different types of complexes due to avoidance of phenyl/(*R*)-NEA steric interactions. In particular, in configurations where keto-carbonyl hydrogen bonding interactions were preferred for MTFP, they are replaced by ester-carbonyl hydrogen bonding interactions for MBF. In this way, the phenyl group of MBF can be placed away from (*R*)-NEA while maintaining the interaction of one or both of the ketoester carbonyls with (*R*)-NEA. With respect to TFAP complexes, the additional carbonyl group in MBF permits the formation of complexes in which strong chemisorption bonding of the phenyl group can

dx.doi.org/10.1021/cs400846j | ACS Catal. 2014, 4, 847−854

occur without incurring a steric repulsion energy cost. The longer ketoester group, as compared to the TFAP acetyl group, permits a variety of binding configurations resulting in lower prochiral selectivity than those observed for TFAP complexes.

AUTHOR INFORMATION

Corresponding Author

*E-mail: peter.mcbreen@chm.ulaval.ca.

Notes

The authors declare no competing financial interest.

ACKNOWLEDGMENTS

The work was supported by NSERC, FQRNT, and the CFI grants. The work was carried out within the FQRNT funded Centre in Green Chemistry and Catalysis. G.G. acknowledges an FQRNT graduate student scholarship.

REFERENCES

(1) (a) Orito, Y.; Imai, S.; Niwa, S. *J. Chem. Soc. Jpn.* **1979**, 1118−1120. (b) Orito, Y.; Imai, S.; Niwa, S. *J. Chem. Soc. Jpn.* **1980**, 670−672.

(2) (a) Sutyinszki, M.; Szori, K.; Felfoldi, K.; Bartok, M. *Catal. Commun.* **2002**, *3*, 125−127. (b) Szollosi, G.; Makra, Z.; Fekete, M.; Fulop, F.; Bartok, M. *Catal. Lett.* **2012**, *142*, 889−894. (c) Schmidt, E.; Mallat, T.; Baiker, A. *J. Catal.* **2010**, *272*, 140−150. (c) Talas, E.; Margitfalvi, J. L.; Egyed, O. *J. Catal.* **2009**, *266*, 191−198. (d) Szöllosi, G.; Cserenyi, S.; Fulop, F.; Bartok, M. *J. Catal.* **2008**, *260*, 245−253. (e) Schmidt, E.; Bucher, C.; Santarossa, G.; Mallat, T.; Gilmour, R.; Baiker, A. *J. Catal.* **2012**, *289*, 238−248. (f) Martin, G.; Maki-Arvela, P.; Murzin, D. Yu.; Salmi, T. *Catal. Lett.* **2013**, *143*, 1051−1060. (g) Balazsik, K.; Bucsi, I.; Cserenyi, S.; Szollosi, G.; Bartok, M. *J. Mol. Catal. A: Chem.* **2008**, *285*, 84−91. (h) Meier, D. M.; Ferri, D.; Mallat, T.; A. Baiker, A. *J. Catal.* **2007**, *248*, 68−76. (i) Maeda, N.; Sano, S.; Mallat, T.; Hungerbühler, K.; Baiker, A. *J. Phys. Chem. C* **2012**, *116*, 4182−4188. (j) Hoxha, F.; Schmidt, E.; Mallat, T.; Schimmoeller, B.; Pratsinis, S. E.; Baiker, A. *J. Catal.* **2011**, *278*, 94−101. (k) Ferri, D.; Bürgi, T.; Baiker, A. *J. Chem. Soc., Perkin Trans.* **2000**, *2*, 221−238. (k) Szollosi, G.; Herman, B.; Fulop, F.; Bartok, M. *React. Kinet. Catal. Lett.* **2006**, *88*, 391−398. (l) Vargas, A.; Reimann, S.; Diezi, S.; Mallat, T.; Baiker, A. *J. Mol. Catal. A: Chem.* **2008**, *282*, 1−8. (m) Balazsik, K.; Szori, K.; Szollosi, G.; Bartok, M. *Catal. Commun.* **2011**, *12*, 1410−1414. (n) Balazsik, K.; Szori, K.; Szollosi, G.; Bartok, M. *Chem. Commun.* **2011**, *47*, 1551−1552.

(3) (a) Maeda, N.; Hungerbühler, K.; Baiker, A. *J. Am. Chem. Soc.* **2011**, *133*, 19567−19569. (b) Mallat, T.; Orglmeister, E.; Baiker, A. *Chem. Rev.* **2007**, *107*, 4863−4890. (c) Bartok, M. *Curr. Org. Chem.* **2007**, *38*, 1533. (d) Blaser, H.-U.; Studer, M. *Acc. Chem. Res.* **2007**, *40*, 1348. (e) Murzin, D. Y.; Mäki-Arvela, P.; Salmi, T. *Catal. Rev: Sci. Eng.* **2005**, *47*, 175. (f) Goubert, G.; McBreen, P. H. *ChemCatChem.* **2013**, *5*, 683. (g) Tálas, E.; Margitfalvi, J. L. *Chirality* **2010**, *22*, 3−15. (h) Kyriakou, G.; Beaumont, S. K.; Lambert, R. M. *Langmuir* **2011**, *27*, 9687. (i) Taskinen, A.; Nieminen, V.; Hotokka, M.; Murzin, D. Y. *J. Phys. Chem. C* **2007**, *111*, 5128. (j) Bonalumi, N.; Bürgi, T.; Baiker, A. *J. Am. Chem. Soc.* **2003**, *125*, 13342. (k) Meemken, F.; Maeda, N.; Hungerbühler, K.; Baiker, A. *Angew. Chem., Int. Ed.* **2012**, *51*, 8212. (l) Baddeley, C.; Jones, T.; Trant, A.; Wilson, K. *Top. Catal.* **2011**, *54*, 1348−1356. (m) Gordon, A. D.; Zaera, F. *Angew Chem. Int. Ed.* **2013**, *52*, 3453. (n) Lavoie, S.; Laliberté, M.-A.; Temprano, I.; McBreen, P. H. *J. Am. Chem. Soc.* **2006**, *128*, 7588−7593. (o) Bonello, J. M.; Williams, F. J.; Lambert, R. M. *J. Am. Chem. Soc.* **2003**, *125*, 2723−2729. (p) Goubert, G.; Demers-Carpentier, V.; Loach, R. P.; Lafleur-Lambert, R.; Lemay, J.-C.; Boukouvalas, J.; McBreen, P. H. *ACS Catal.* **2013**, *3*, 2677−2683.

(4) Demers-Carpentier, V.; Goubert, G.; Masini, F.; Lafleur-Lambert, R.; Dong, Y.; Lavoie, S.; Mahieu, G.; Boukouvalas, J.; Gao, H.; Rasmussen, A. M. H.; Ferrighi, L.; Pan, Y.; Hammer, B.; McBreen, P. H. *Science* **2011**, *334*, 776−780.

(5) Demers-Carpentier, V.; Rasmussen, A. M. H.; Goubert, G.; Ferrighi, L.; Masini, F.; Dong, Y.; Lemay, J.-C.; Masini, F.; Zeng, Y.; Hammer, B.; McBreen, P. H. *J. Am. Chem. Soc.* **2013**, *135*, 9999−10002.

(6) (a) Burkholder, L.; Garvey, M.; Weinert, M.; Tysoe, W. T. *J. Phys. Chem. C* **2011**, *115*, 8790−8797. (b) Boscoboinik, J. A.; Bai, Y.; Burkholder, L.; Tysoe, W. T. *J. Phys. Chem. C* **2011**, *115*, 16488−16494.

(7) Horcas, I.; Fernandez, R.; Gomez-Rodriguez, J. M.; Colchero, J.; Gomez-Herrero, J.; Baro, A. M. *Rev. Sci. Instrum.* **2007**, *78*, 013705.

(8) Vargas, A.; Reimann, S.; Diezi, S.; Mallat, T.; Baiker, A. *J. Mol. Catal. A: Chem.* **2008**, *282*, 1−8.

(9) (a) Rasmussen, A. M. H.; Hammer, B. *J. Chem. Phys.* **2012**, *136*, 174706−174709. (b) Goubert, G.; Rasmussen, A. M. H.; Dong, Y.; Groves, M. N.; McBreen, P. H.; Hammer, B. submitted for publication.

(10) Schmidt, E.; Mallat, T.; Baiker, A. *J. Catal.* **2010**, *272*, 140−150.

(11) Cakl, Z.; Reimann, S.; Schmidt, E.; Moreno, A.; Mallat, T.; Baiker, A. *J. Catal.* **2011**, *280*, 104−115.